Object discrimination and orientation determination in speckled images

Jihad S. Daba
Mark R. Bell, MEMBER SPIE
Purdue University
School of Electrical Engineering
West Lafayette, Indiana 47907-1285

Abstract. Detection and identification of objects in images formed by coherent imaging systems are complicated by the presence of speckle. Speckle not only complicates these problems for human observers, but also for machine detection and identification algorithms. We investigate optimal statistical tests for object discrimination and orientation determination in speckle and compare their performance to that of human observers for the same problems. We formulate maximum likelihood tests for determining the orientation of an object and for discriminating among a set of known objects in a speckled image. We then analyze the performance of these tests to study the system requirements for reliable object discrimination and orientation determination. Next we generalize these tests and their corresponding performance analyses into three broad classes of pattern recognition problems, corresponding to orthogonal, antipodal, and biorthogonal signal problems in statistical communications theory. These generalizations make the design and analysis of a broad range of object discrimination and orientation determination straightforward. Finally we compare the performance of these tests to the results of Korwar and Pierce for human interpretation of objects in speckled images. We note that for fixed image contrast, number of looks, and image size in pixels, object shape has no effect on machine detection performance. This is not true for the human observer.

Subject terms: speckle; synthetic aperture radar; pattern recognition.

Optical Engineering 33(4), 1287–1302 (April 1994).

1 Introduction

Speckle noise, which is a form of object- or target-induced random noise, is present whenever coherent radiation is employed to image an object, surface, or scene and can be observed in coherent imaging systems such as synthetic aperture radar (SAR), which employs coherent microwave illumination,[1] ultrasonic imaging systems that use coherent acoustic illumination,[2–4] laser and sonar imaging systems, and interferometry and holography.[5]

Speckle arises from the interference of dephased coherent wavefronts scattered from a diffusely reflecting surface that is rough on the wavelength scale of the illuminating radiation. This interference produces bright and dark areas that are superimposed on the image as a random granular pattern known as speckle.[6] The speckle effect, however, masks small to moderate differences in the average image reflectivity presented by gray levels, and so reduces the radiometric resolution capabilities of the imaging systems and the amount of information available in the speckled images.[7,8] Speckle thus complicates the detection and identification of objects in speckled images for human observers and also for the related machine detection problems.

In the literature, extensive work has been done on reducing speckle to minimize its visual degradation of images through filtering techniques.[9–11] Relatively little work has been done on the effects of speckle in detection and pattern recognition problems (object discrimination and orientation determination) for speckled images. Notable exceptions include Ref. 12, in which the determination of object boundaries in speckle is considered, and in which the segmentation of speckled SAR images using a Markov random field model is considered.[13,14] These problems are of special interest in terrain mapping and analysis by SAR systems. They are also equally important in image analysis problems in speckle as it arises in other coherent imaging systems, such as acoustic speckle in biomedical ultrasound imaging systems.

We are interested in studying the problems of detection in images corrupted by speckle, with an emphasis on speckle as it arises in SAR systems. We use SAR systems in our analysis to establish results that will serve as a basis for detection problems in other coherent imaging systems where the speckle phenomenon is present, such as ultrasonic, sonar, and laser imaging systems. For example, since acoustic speckle can be treated in a similar way as laser speckle,[2] the assumptions made about speckle in SAR images could also be made about speckle in acoustic images obtained with ultrasonic medical imaging systems, such as ultrasound B-mode scanners.[3,4]

Synthetic aperture radar data is reviewed by geoscientists, oceanographers, agronomists, and cartographers who want to perform object detection, pattern recognition, and other information extraction from SAR images. With the recent

Paper 21053 received May 22, 1993; revised manuscript received Oct. 9, 1993; accepted for publication Oct. 10, 1993.

increase in the volume of SAR data collected and the resulting complexity of data analysis by humans, the role of automated SAR image analysis, by developing machine related detection techniques and implementing them on digital computers, has become increasingly important. As a result, a better understanding of the optimal statistical tests for object detection in SAR images is crucial. The detection problem for human observers has been studied by Korwar and Pierce.[15,16] Our interest lies in the related machine detection problems.

In this paper, we formulate optimal statistical tests for the pattern recognition problems of object orientation and discrimination among a set of known object forms in SAR images, assuming a fully developed model. We then analyze the performance of these tests. The system requirements for reliable object discrimination and orientation determination are studied by calculating the probability of error as a function of the number of SAR looks, the image contrast ratio, and the size (in pixels) of the object being considered. We then generalize the form of the optimal tests and their corresponding error analyses for pattern recognition problems into three classes corresponding to orthogonal, antipodal, and biorthogonal signal detection problems in statistical communication theory. Finally, we compare the optimal statistical tests performance for machine detection of SAR images to that of the human visual system studied by Korwar and Pierce.[15,16]

2 Speckle Model

2.1 *Single-Look Model*

Surfaces imaged by radar and other coherent imaging systems have varying degrees of surface roughness with respect to the wavelength of the illuminating radiation. This roughness can be viewed in terms of the locations of the individual scatterers or scattering centers that contribute to the radar backscatter from the surface.[17] When the number of scatterers within a surface resolution cell is very large, and their distribution in height occurs on a scale of a wavelength or greater, the speckle is referred to as *fully developed.*[6] For fully developed speckle, the size of the individual speckle granules is determined by the resolution cell size of the imaging system.

Fully developed speckle arises from the coherent sum of the scattered electric fields from a large number N of elemental scatterers making up a rough surface resolution cell, according to

$$I=\left|\sum_{j=1}^{N} A_j \exp(i\phi_j)\right|^2 , \tag{1}$$

where A_j and ϕ_j are the reflectance strength (or size) and phase of the j'th elementary scatterer. It is commonly assumed that the elementary scatterer amplitudes are statistically independent, that the spatial location of a particular scatterer (and hence its phase) is statistically independent of the positions (phases) of all other individual scatterers, and that elementary scatterers sizes are independent of scatterers positions. It is also commonly assumed that the phases of the fields scattered by the elemental scatterers are uniformly distributed[1] over the interval $[0, 2\pi)$. In the limit of a large number of independent scattered contributions for fully developed speckle, it follows from the central limit theorem[18] that the in-phase and quadrature components of the total received electric field are zero mean, identically distributed, and uncorrelated Gaussians. It follows then that the probability density function of the intensity I, defined as the sum of the squares of these components, has an exponential distribution given by

$$p_I(I)=\frac{1}{\mu}\exp\left(-\frac{I}{\mu}\right)I_{[0,\infty)}(I) . \tag{2}$$

Here $I_A(\cdot)$ is the indicator function, defined as

$$I_A(x)=\begin{cases}1 & \text{if } x\in A,\\ 0 & \text{if } x\notin A,\end{cases} \tag{3}$$

and μ is the mean intensity (or reflectivity) of the field reflected from the observed resolution cell.

The conditions mentioned earlier under which the speckle intensity is exponentially distributed are fairly weak. The inphase and quadrature phase components of the elementary scatterers were assumed to be statistically independent for the central limit theorem to apply. However, this need not be the case, as it can be shown that the sum of a sequence of dependent random variables can still be asymptotically Gaussian under relatively weak conditions.[19]

The statistics of fully developed speckle are studied in detail by Goodman.[6] This speckle model is widely used in radar imaging. An exponential model for radar reflectivity is also widely used for modeling the scattering characteristics of complex targets. For example, the Swerling I and Swerling III models commonly used in radar systems analysis assume that the intensity of the total scattered field is exponentially distributed.

2.2 *Multilook Model*

Many speckle reduction methods are presented in the literature using filtering techniques.[9–11] One common speckle reduction technique involves the noncoherent sum of L statistically independent looks at each intensity pixel as

$$I_L=\sum_{k=1}^{L} i_k , \tag{4}$$

where i_k is the k'th look measured intensity over a pixel. The intensity I_L in this case obeys a gamma distribution (Ref. 6, pp. 21–24):

$$p_{I_L}(I_L)=\frac{I_L^{L-1}\exp(-I_L/\mu)}{\mu^L\Gamma(L)}I_{[0,\infty)}(I_L) , \tag{5}$$

where $\Gamma(\cdot)$ is the gamma function defined as

$$\Gamma(\alpha)=\int_0^{\infty} t^{\alpha-1}\exp(-t)\,dt, \quad \alpha>0. \tag{6}$$

The argument for the speckle reduction by the noncoherent averaging of intensities over a pixel is made by considering the signal-to-noise ratio (SNR) of the image. The speckle contrast for a fully developed speckle is defined by $c=\sigma_{I_L}/\mu$, where σ_{I_L} is the standard deviation of the intensity based on L looks. Goodman[6] suggests that a good measure of the SNR is $1/c$. For a single look, c is unity because $\sigma_{I_L}=\mu$ for the exponential distribution. As we increase the number of looks to L, the SNR $1/c$ increases by a factor of $\sqrt{L}$. Thus, the effect of image degradation resulting from speckle is decreased by increasing L, as reflected by the increase in SNR. Note also that for L independent looks, I_L is a complete sufficient statistic for μ, and thus $\hat{\mu}=I_L/L$ is the minimum variance unbiased estimator (MVUE) and the maximum likelihood (ML) estimate of the unknown parameter μ.

In practice, many techniques in SAR are employed to obtain multilook images. Methods of obtaining multiple looks include using multiple carrier frequencies, observing the surface from different positions, and considering continuous resolution cells in range or azimuth to come from a homogeneous region of the surface and considering their intensities to be independent measurements of the surface reflectivity in that region.[20] Multilook images can be obtained in other coherent imaging systems by simply varying the proper control parameters of the scanning device from frame to frame, and averaging the resulting L sequential uncorrelated frames of the same image.[2] In SAR, a trade-off exists between the number of looks L and the contrast ratio. In reality, when SAR data are processed, the receiver performs a 2-D match filtering of the signal returns, which causes an increase in the integrated sidelobe ratio of the autocorrelation function of the filter impulse response, and hence reduces the contrast ratio of the image. In addition, spatial resolution is also sacrificed with an increase of number of looks. Nevertheless, very little information is contained in a single-look pixel,[21,22] and it is often beneficial to increase the number of looks at the cost of sacrificing some resolution.[7,15,23]

3 Pattern Recognition Problems

3.1 *The Image Model*

We consider an object to be a binary image, that is, a 2-D pattern of pixels, each pixel taking on one of two possible average reflectivities μ_0 or μ_1 ($\mu_1>\mu_0$) with a contrast ratio $r=\mu_1/\mu_0$. While the assumption of a binary reflectivity-image model introduces a significant simplification over what may be encountered in real speckled images, it allows for the analytical investigation of the effect of speckle in discrimination problems. Furthermore, it has been shown that even in speckled images where the underlying surface can take on a continuum of reflectivity values, the mutual information between the reflectivity and a single speckle intensity measurement is approximately 1 bit per resolution cell.[21,22] Hence, the maximum number of reflectance levels that a single resolution cell could be assigned with statistical reliability based on a single intensity observation is two. So in terms of analyzing object discrimination in speckle, the binary reflectance-image model is not as great a simplification as it may initially seem. It is not uncommon in SAR images to assume that pixel boundaries are exactly aligned with object boundaries, and hence focus on the structure of the object (assumed to have been already located) by neglecting the effect of the background. Also, if the image is sampled coarsely enough so that the pixel spacing is approximately equal to the resolution cell size to avoid the introduction of small correlations between neighboring pixels, the speckle intensity can be assumed to be conditionally independent from pixel to pixel[12,24] conditioned on the reflectivity (average intensity) assumed constant within each pixel. The image model also assumes that each intensity pixel has fully developed speckle, and that L independent diversity measurements (SAR looks) of each pixel are made.

We seek to develop optimal statistical tests based on these measurements for the two problems: determination of the orientation of a single object and object form discrimination (discriminating among different patterns of an object). The analysis is later extended to the problem of object orientation-determination and form discrimination from a set of K object patterns.

3.2 *Grating Orientation*

3.2.1 *Overview*

Consider a grating with lines one resolution cell wide and having lines of alternating pixel intensities μ_0 (dark) and μ_1 (bright). The grating consists of a total of $M\times N$ resolution cells (M rows, N columns) as shown in Fig. 1.

The problem is to detect two possible orientations of the grating: vertical (hypothesis H_0) versus horizontal (hypothesis H_1). The grating model is considered because of the multiple frequency components in its pattern, which makes it a good detection problem to study human interpretation of objects in speckle as a result of the frequency response of the human visual system. This model was considered by Korwar and Pierce[15,16] in the psychological detection experiments they conducted on human observers. We consider this model to compare the results of machine detection to those obtained from human observers. In addition, as we show later, the results obtained from this simple model can be generalized to gratings with lines that are d pixels wide, and more importantly, to more complex object orientation problems.

3.2.2 *Maximum likelihood decision rule*

We consider an ML parametric detection test $\phi(\cdot)$ defined as

$$\phi(\mathbf{I})=\begin{cases}1 & \text{if } L(\mathbf{I})>\lambda \ (H_1)\\ 0 & \text{if } L(\mathbf{I})<\lambda \ (H_0)\end{cases}, \tag{7}$$

where the likelihood ratio $L(\mathbf{I})$ is given by

$$L(\mathbf{I})=\frac{p(\mathbf{I}|H_1)}{p(\mathbf{I}|H_0)}, \tag{8}$$

and the threshold λ is unity for both optimal ML detection and Bayesian detection under the assumptions that the *a priori* probability of each hypothesis is equal to ½ and that the cost C_{ij} of deciding H_i when H_j is true equals the

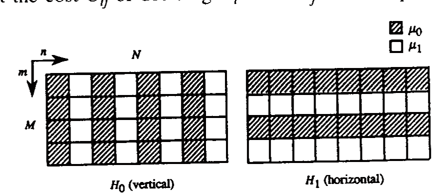

Fig. 1 Orientation detection of a grating with $M\times N$ intensity pixels and lines one resolution cell wide.

Kronecker delta function[25] δ_{ij}. The image is described by a lexicographic ordered vector of pixel intensities $\mathbf{I}=(I_{11},I_{12},\ldots,I_{MN})$. Let μ_n denote one of the two values μ_0 and μ_1 that the reflectivity can take over the n'th column. Using the probability density function (pdf) of a pixel intensity based on L looks in Eq. (5) and assuming that the pixel intensities are statistically independent conditioned on their average intensities, the joint pdf of the intensities conditioned on H_0 is

$$p_0(\mathbf{I})=\prod_{n=1}^{N}\prod_{m=1}^{M}\left[\frac{I_{mn}^{L-1}\exp(-I_{mn}/\mu_n)}{\mu_n^L(L-1)!}I_{[0,\infty)}(I_{mn})\right]$$
$$=\prod_{n\ \mathrm{odd}}\left\{\frac{1}{\mu_0^{ML}[(L-1)!]^M}\times\exp\left(-\frac{1}{\mu_0}\sum_{m=1}^{M}I_{mn}\right)\left(\prod_{m=1}^{M}I_{mn}^{L-1}\right)\right\}$$
$$\times\prod_{n\ \mathrm{even}}\left\{\frac{1}{\mu_1^{ML}[(L-1)!]^M}\times\exp\left(-\frac{1}{\mu_1}\sum_{m=1}^{M}I_{mn}\right)\left(\prod_{m=1}^{M}I_{mn}^{L-1}\right)\right\}$$
$$\times I_{[0,\infty)}(\min\{I_{mn}\})\ . \qquad (9)$$

For the case when N is even, there are $N/2$ vertical columns with reflectivity μ_0 and $N/2$ vertical columns with reflectivity μ_1. When N is odd, there are $(N+1)/2$ horizontal rows with reflectivity μ_0 and $(N-1)/2$ horizontal rows with reflectivity μ_1. Equation (9) simplifies to

$$p_0(\mathbf{I})=\frac{1}{B}\exp\left(-\frac{1}{\mu_0}\sum_{n\ \mathrm{odd}}\sum_{m=1}^{M}I_{mn}\right)\times\exp\left(-\frac{1}{\mu_1}\sum_{n\ \mathrm{even}}\sum_{m=1}^{M}I_{mn}\right)\times\left(\prod_{n=1}^{N}\prod_{m=1}^{M}I_{mn}^{L-1}\right)I_{[0,\infty)}(\min\{I_{mn}\})\ , \qquad (10)$$

where B is a constant taking on values of $(\mu_1\mu_0)^{MNL/2}[(L-1)!]^{MN}$ when N is even and $\mu_1^{M(N-1)L/2}\mu_0^{M(N+1)L/2}[(L-1)!]^{MN}$ when N is odd. The joint pdf of the intensities conditioned on H_1 has the same form as Eq. (10). From the symmetry of the problem, by interchanging m and n and M and N, we obtain the following expression for the joint pdf of the intensities conditioned on H_1:

$$p_1(\mathbf{I})=\frac{1}{B}\exp\left(-\frac{1}{\mu_0}\sum_{m\ \mathrm{odd}}\sum_{n=1}^{N}I_{mn}\right)\times\exp\left(-\frac{1}{\mu_1}\sum_{m\ \mathrm{even}}\sum_{n=1}^{N}I_{mn}\right)\times\left(\prod_{m=1}^{M}\prod_{n=1}^{N}I_{mn}^{L-1}\right)I_{[0,\infty)}(\min\{I_{mn}\})\ , \qquad (11)$$

with B having the values $(\mu_1\mu_0)^{MNL/2}[(L-1)!]^{MN}$ when M is even and $\mu_1^{N(M-1)L/2}\mu_0^{N(M+1)L/2}[(L-1)!]^{MN}$ when M is odd.

Applying the likelihood ratio test of Eqs. (7) and (8) results in the test

$$\frac{p_1(\mathbf{I})}{p_0(\mathbf{I})}\ \underset{H_0}{\overset{H_1}{\gtrless}}\ 1\ . \qquad (12)$$

Substituting Eqs. (10) and (11) into Eq. (12) and taking the logarithm of both sides, we obtain

$$C\ \ln(r)-\frac{1}{\mu_0}I^*+\frac{1}{\mu_1}I^*\ \underset{H_0}{\overset{H_1}{\gtrless}}\ 0\ , \qquad (13)$$

where the statistic I^* is

$$I^*=\sum_{m\ \mathrm{odd}}\sum_{n\ \mathrm{even}}I_{mn}-\sum_{m\ \mathrm{even}}\sum_{n\ \mathrm{odd}}I_{mn}\ , \qquad (14)$$

the contrast ratio $r=\mu_1/\mu_0$, $(\mu_1>\mu_0)$, and C is a constant given in Table 1.

Table 1 Values of the constants C, ν, and η.

M \ N	even			odd		
	C	ν	η	C	ν	η
even	0	$\frac{MNL}{4}$	$\frac{MNL}{4}$	$\frac{-ML}{2}$	$\frac{M(N-1)L}{4}$	$\frac{M(N+1)L}{4}$
odd	$\frac{NL}{2}$	$\frac{(M+1)NL}{4}$	$\frac{(M-1)NL}{4}$	$\frac{(N-M)L}{2}$	$\frac{(M+1)(N-1)L}{4}$	$\frac{(M-1)(N+1)L}{4}$

Further simplification of Eq. (13) yields the decision rule for the detection test as

$$I^* \underset{H_1}{\overset{H_0}{\gtrless}} I_t \,, \tag{15}$$

where the decision threshold I_t is given by

$$I_t = \frac{C \ln(r)}{(1/\mu_0)-(1/\mu_1)} \,. \tag{16}$$

Even though this decision rule applies only to the two patterns shown in Fig. 1, where column 1 (vertical grating) and row 1 (horizontal grating) are dark pixels, we will show later that the same decision rule could be used regardless of the arrangements of dark and bright pixels in the two patterns.

Examination of the statistic I^* in Eq. (14) shows that the pixels (m,n) with both m and n simultaneously even or simultaneously odd do not contribute to I^* and hence are not used in decision making. The fact that half of the data is not used is justified intuitively by superimposing the grid under H_0 on top of the grid under H_1 and noticing that only the differing pixels will affect the decision rule. The greater the number of differing pixels between the two grids, the more easily they can be discriminated.

In Appendix A, we show that the conditional pdf of I^* is given by

$$p_0(I^*) = \mu_1^{-\nu}\mu_0^{-\eta}\left[\sum_{k=0}^{\nu-1} a_k I^{*k} \exp(-I^*/\mu_1) I_{[0,\infty)}(I^*) + \sum_{k=0}^{\eta-1} b_k(-I^*)^k \exp(I^*/\mu_0) I_{(-\infty,0)}(I^*)\right] \,, \tag{17}$$

where

$$a_k = \frac{1}{k!}\binom{\eta+\nu-k-2}{\eta-1}\left(\frac{1}{\mu_1}+\frac{1}{\mu_0}\right)^{-\eta-\nu+k+1} \,, \tag{18}$$

$$b_k = \frac{1}{k!}\binom{\eta+\nu-k-2}{\nu-1}\left(\frac{1}{\mu_1}+\frac{1}{\mu_0}\right)^{-\eta-\nu+k+1} \,, \tag{19}$$

and the constants η and ν are given in Table 1. Note from Table 1 that $C=\nu-\eta$. The expression for the conditional pdf $p_1(I^*)$ is obtained by interchanging μ_0 and μ_1 in Eqs. (17), (18), and (19).

We now consider the probability of decision error for this problem. The probability of error for the test $\phi(\cdot)$ is[25]

$$P_e = \frac{1}{2}\{Pr[\phi(\mathbf{I})=1|H_0] + Pr[\phi(\mathbf{I})=0|H_1]\} \,, \tag{20}$$

or, after using the decision rule in Eqs. (15) and (16),

$$P_e = \frac{1}{2}[Pr(I^* < I_t|H_0) + Pr(I^* > I_t|H_1)] \,. \tag{21}$$

Using the expressions in Eqs. (17), (18), and (19) for the pdf $p_0(I^*)$ under the hypothesis H_0 and the dual expression for the pdf $p_1(I^*)$ under the hypothesis H_1, and applying Eq. (21), we show in Appendix B that the final expression for the probability of error is given by

$$\begin{aligned} P_e = \frac{1}{2}\Bigg\{ & (1+r)^{-\eta}\sum_{k=0}^{\nu-1}\binom{\eta+k-1}{\eta-1} \times (1+r^{-1})^{\nu-k} Q_{\nu-k}\left\{0,\left[\frac{2\ln(r)|\nu-\eta|}{1-r^{-1}}\right]^{1/2}\right\} \\ & + (1+r^{-1})^{-\eta}\sum_{k=0}^{\nu-1}\binom{\eta+k-1}{\eta-1} \times (1+r)^{\nu-k}\left(1-Q_{\nu-k}\left\{0,\left[\frac{2\ln(r)|\nu-\eta|}{r-1}\right]^{1/2}\right\}\right) \\ & + (1+r)^{-\nu}\sum_{k=0}^{\eta-1}\binom{\nu+k-1}{\nu-1}(1+r^{-1})^{\eta-k}\Bigg\} \end{aligned} \tag{22}$$

for $\nu \geq \eta$, and

$$\begin{aligned} P_e = \frac{1}{2}\Bigg\{ & (1+r)^{-\nu}\sum_{k=0}^{\eta-1}\binom{\nu+k-1}{\nu-1} \times (1+r^{-1})^{\eta-k} Q_{\eta-k}\left\{0,\left[\frac{2\ln(r)|\nu-\eta|}{1-r^{-1}}\right]^{1/2}\right\} \\ & + (1+r^{-1})^{-\nu}\sum_{k=0}^{\eta-1}\binom{\nu+k-1}{\nu-1} \times (1+r)^{\eta-k}\left(1-Q_{\eta-k}\left\{0,\left[\frac{2\ln(r)|\nu-\eta|}{r-1}\right]^{1/2}\right\}\right) \\ & + (1+r)^{-\eta}\sum_{k=0}^{\nu-1}\binom{\eta+k-1}{\eta-1}(1+r^{-1})^{\nu-k}\Bigg\} \end{aligned} \tag{23}$$

for $\nu < \eta$. Here the function $Q_N(\alpha,\beta)$ is the generalized Marcum Q-function that is frequently used in signal detection problems.[26–28] The definition of $Q_N(\alpha,\beta)$ can be found in Appendix B.

For the case where $\nu=\eta$, the threshold intensity $I_t=0$, and the generalized Marcum Q-function is unity in Eq. (22), as its argument is zero. Equation (22) then simplifies to

$$P_e = (2+r+r^{-1})^{-\nu}\sum_{j=0}^{\nu-1}\begin{bmatrix}2(\nu-1)-j\\ \nu-1\end{bmatrix}(1+r^{-1})^{j+1} \tag{24}$$

after making the change of variable $j=\nu-1-k$ in Eq. (22). Equation (24) is consistent with an error probability formula obtained by Bovik and Munson[12] for the problem of detecting object boundaries in speckle.

Equations (22) and (23) relate the probability of error to the number of looks L, the image contrast ratio r, and the size in resolution cells (M and N) of the object being considered (ν and η are functions of L, M, and N). These equations make the design of optimal detectors for object orientation problems straightforward. For example, it is not difficult to find the number of looks required to produce 95% probability of correct detection for the orientation of an object with a 3-dB contrast ratio and 10×10 pixels in size.

As shown in Fig. 2, P_e decreases with a higher contrast ratio r for a fixed number of looks L and object size (M and N). Note also from Fig. 2 that P_e decreases with r at a faster rate for a larger value of L. Figure 3 shows that an increase in object size M and N decreases P_e for fixed values of L and r. The rate of decrease is greater for larger values of L. Thus, it is not possible to characterize the detector performance by a single parameter. For a fixed r, increasing the object size and the number of looks will result in a lower probability of error. Note that the probability of error decreases with an increase in the parameters ν and η, which are proportional to the number of SAR looks L and to the number of differing pixels between the two gratings under the hypotheses H_0 and H_1. This is in agreement with the intuitive notion that the object orientations become more easily discriminated as the difference between the alternative orientation patterns becomes larger.

3.2.3 *Grating orientation with lines* d *pixels wide*

We now consider the more general case of a grating with lines that are d resolution cells wide as shown in Fig. 4. The grating still consists of a total of $M\times N$ resolution cells, with M and N being integer multiples of d; that is, $M=ld$ and $N=qd$, where l and q are positive integers.

Following the same analytical approach as Sec. 3.2.2, we obtain the same decision rule as in Eqs. (15) and (16), where the statistic I^* is now

$$I^*=\sum_{k=1,\mathrm{odd}}^{l}\ \sum_{m=(k-1)d+1}^{kd}\ \sum_{j=1,\mathrm{even}}^{q}\ \sum_{n=(j-1)d+1}^{jd} I_{mn} - \sum_{k=2,\mathrm{even}}^{l}\ \sum_{m=(k-1)d+1}^{kd}\ \sum_{j=1,\mathrm{odd}}^{q}\ \sum_{n=(j-1)d+1}^{jd} I_{mn}\ , \tag{25}$$

and the constant C in Eq. (16) is given in Table 1 after replacing M and N in the left upper corner by l and q, respectively. Again, we note that, like the previous grating orientation problem, only half of the data is used in decision making, and that only the different pixels components between the two hypotheses contribute to I^* and affect the decision rule. The decision criteria is best illustrated in Fig. 5.

The same analysis of Section 3.2.2 yields the same expressions for the probability of error P_e as in Eqs. (22) and (23), with the constants ν and η having values as given in Table 1, except that M and N in the left upper corner are replaced by l and q, respectively. In addition to the quantitative analysis of the error probability equations that was provided in Sec. 3.2.2, we note that P_e is independent of the grating line width d. Thus, for a fixed object size M and N (in resolution cells), a fixed contrast ratio r, and the same number of SAR looks

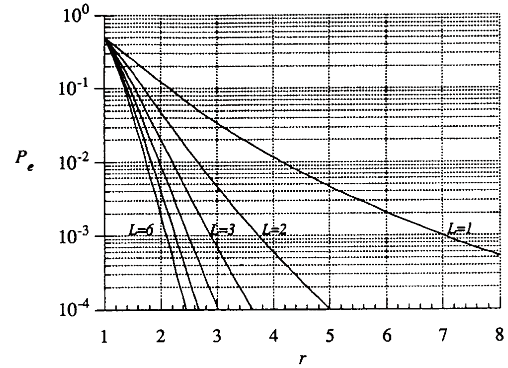

Fig. 2 Probability of error for the optimal detection of grating orientation versus the contrast ratio r, for $M=N=5$.

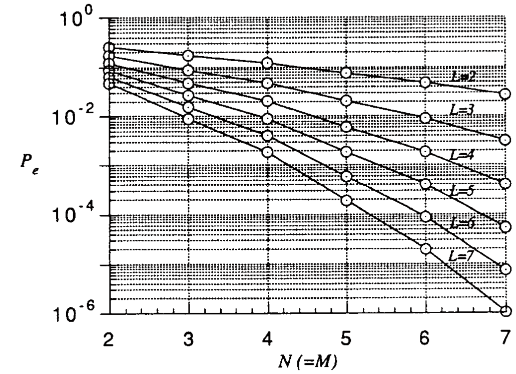

Fig. 3 Probability of error for the optimal detection of grating orientation versus the object size $M(N)$. The contrast ratio r is fixed at 2.0.

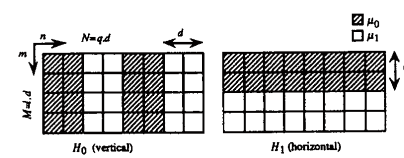

Fig. 4 Orientation detection of a grating with lines d pixels wide.

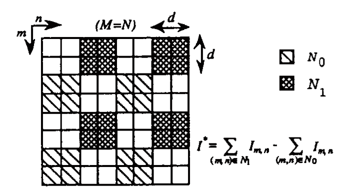

Fig. 5 The decision rule for grating orientation detection.

L, the detector has the same performance regardless of the line thickness d. For example, the grating orientation problems of Fig. 4($d=2$) and Fig. 1 ($d=1$) have the same probability of error. Intuitively, we can explain the fact that P_e does not decrease with wider grating lines by noting that an increase in line thickness d reduces the number of grating lines, and vice versa, keeping the total number of bright (μ_1) and dark (μ_0) pixels fixed. This interesting result only applies to machine detection. For the human visual system, grating orientation in speckle is more easily discriminated when the grating lines increase in width.[16]

3.3 *Pattern Discrimination*

The detection problem under consideration is the discrimination between two alternative image forms (the term *forms* refers to distinct binary image patterns). We consider the forms of set 1 (shapes "E" versus "F" in Fig. 6) in our derivation, although the same analysis can be applied to other forms (such as sets 2 and 3). Let μ_{mn} denote one of the two values μ_0 and μ_1 that the reflectivity can take over the (m,n) pixel in the image.

Applying the likelihood ratio test of Eqs. (7) and (8) and using the conditional independence of the intensity pixels $\{I_{mn}\}$, we obtain

$$\frac{p_1(\mathbf{I})}{p_0(\mathbf{I})}=\frac{\prod_{(m,n)\in N_1} p(I_{mn}|\mu_0)\prod_{(m,n)\in N_1^c} p(I_{mn}|\mu_{mn})}{\prod_{(m,n)\in N_1} p(I_{mn}|\mu_1)\prod_{(m,n)\in N_1^c} p(I_{mn}|\mu_{mn})}\underset{H_0}{\overset{H_1}{\gtrless}} 1 , \tag{26}$$

where the set N_1, shown in Fig. 6 (the rightmost two pixels in the last row), is the set of pixels that differ between the two forms, and N_1^c is its complement. Using the pdf of an intensity pixel I_{mn} based on L looks given in Eq. (5),

$$\frac{p_1(\mathbf{I})}{p_0(\mathbf{I})}=\left(\frac{\mu_1}{\mu_0}\right)^{\nu}\frac{\exp\left(-\frac{1}{\mu_0}\sum_{(m,n)\in N_1} I_{mn}\right)}{\exp\left(-\frac{1}{\mu_1}\sum_{(m,n)\in N_1} I_{mn}\right)}\underset{H_0}{\overset{H_1}{\gtrless}} 1 , \tag{27}$$

where $\nu=L\times\mathrm{card}(N_1)$, with card (N_1) (cardinality of N_1) being the number of pixel elements in the set N_1. Taking the logarithm of both sides of the inequalities yields the following decision rule

$$I^* \underset{H_1}{\overset{H_0}{\gtrless}} I_t , \tag{28}$$

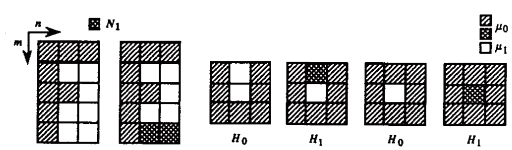

Fig. 6 Discrimination between two alternative forms.

with the statistic

$$I^*=\sum_{(m,n)\in N_1} I_{mn} , \tag{29}$$

and the decision threshold

$$I_t=\frac{\nu\ \ln(r)}{(1/\mu_0)-(1/\mu_1)} . \tag{30}$$

The conditional pdf $p_0(I^*)$ of I^* conditioned on H_0 is given by

$$p_0(I^*)=\frac{I^{*\nu-1}\exp(-I^*/\mu_1)}{\mu_1^{\nu}\Gamma(\nu)}I_{[0,\infty)}(I^*) , \tag{31}$$

and $p_1(I^*)$ is given by the same expression with μ_1 replaced by μ_0. Note that the way in which H_0 and H_1 are defined in Fig. 6 dictates the fact that the pixels in N_1 have average intensity μ_1 when H_0 is true and μ_0 when H_1 is true. This is why $p_0(I^*)$ has parameter μ_1 and $p_1(I^*)$ has parameter μ_0. Substituting the conditional pdfs of I^* into the probability of error expression of Eq. (21), and using the definite integral formula of Eq. (66) in Appendix B results in the final expression for P_e:

$$P_e=\frac{1}{2}\left(1-Q_{\nu}\left\{0,\left[\frac{2\nu\ \ln(r)}{r-1}\right]^{1/2}\right\}+Q_{\nu}\left\{0,\left[\frac{2\nu\ \ln(r)}{1-r^{-1}}\right]^{1/2}\right\}\right) . \tag{32}$$

The probability of error P_e in Eq. (32) is a decreasing function of the image contrast ratio r, the number of looks L, and the number of differing pixels card(N_1) between the two alternative forms. The probability of error is independent of the intensity pixels in the set N_1^c; therefore, for fixed L and r, the probability of error for form discrimination is the same for different sets of alternative forms having an equal number of differing pixels [card(N_1)]. For example, the detection test has the same performance for sets 2 and 3 in Fig. 6, which means that the shape of the object has no effect on machine detection performance. This result is not true for human visual detection.[15]

4 Classification of Pattern Recognition Problems

Based on the analyses of the detection problems of grating orientation and form discrimination, we classify a broad range of general pattern recognition problems into three categories: Type I, II, and III. We then show that these three classes of problems correspond to orthogonal, antipodal, and biorthogonal signal detection problems in statistical communication theory, respectively. This correspondence will be emphasized in this section to establish results for general pattern recognition problems by using the well-established theory of signal detection at the receiver end of a communication channel.

4.1 *Type I Problems*

Type I problems correspond to orthogonal signaling problems in statistical communication theory. Both orientation-determination [Fig. 7(a)] and pattern discrimination problems [Fig. 7(b)] can fall into the Type I problem category.

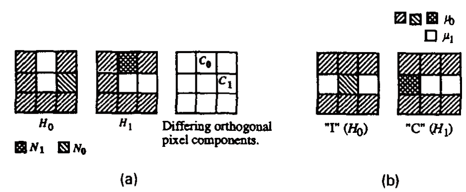

Fig. 7 (a) Two alternative orientations of a pattern and (b) discrimination between two alternative shapes ("I" versus "C").

The grid orientation problem of Sec. 3.2 is considered to be a Type I problem. In Type I problems, we consider an object with individual pixels taking on two reflectivity levels μ_0 and μ_1 ($\mu_1 > \mu_0$) under two hypotheses H_0 and H_1. We define the sets N_1 and N_0, neither of which is empty, as follows: $N_1 = \{(m,n)$ dark pixels (μ_0) under H_1 that are different from the dark pixels under $H_0\}$, and $N_0 = \{(m,n)$ dark pixels under H_0 that are different from the dark pixels under $H_1\}$. Let $\nu = \mathrm{card}(N_1) \times L$ and $\eta = \mathrm{card}(N_0) \times L$, where L is the number of SAR looks. The number of pixels in the set N_i(card (N_i)) is equal to the area of the N_i region divided by the resolution limit area.

Based on the analysis of Sec. 3.2.2, we obtain a decision rule for the maximum likelihood test as in Eqs. (15) and (16), where the statistic I^* is now

$$I^* = \sum_{(m,n)\in N_1} I_{mn} - \sum_{(m,n)\in N_0} I_{mn} \; . \tag{33}$$

It follows that the probability of error P_e is the same as in Eqs. (22) and (23).

4.1.1 *Analogy to binary orthogonal signals*

Consider the Type I detection problem in Fig. 7(a). There are two different components C_0 and C_1 between the hypotheses H_0 and H_1, which we refer to as *orthogonal* components. For the case when card $(N_1) = \mathrm{card}(N_0)$ (or $\nu = \eta$), we claim that the detection problem is equivalent to the optimal detection of equal-energy binary orthogonal signals at the receiver end of a communication channel with additive noise.

Given a set of K equally likely equal-energy binary orthogonal signals $\{C_i, i = 0, \ldots, K-1\}$, the probability of correct detection given that C_0 is transmitted[29,30] is given by

$$P_{c|C_0} = \int_{-\infty}^{\infty} p_{H_0}(\alpha)\left[\int_{-\infty}^{\alpha} p_{H_1}(\beta)\, \mathrm{d}\beta\right]^{K-1} \mathrm{d}\alpha \; , \tag{34}$$

where H_i denotes the received signal. The probability of correct detection is given by

$$P_c = \frac{1}{K}\sum_{i=0}^{K-1} P_{c|C_i} \; , \tag{35}$$

and since $P_{c|C_i} = P_{c|C_j}$ from the symmetry of the problem, it follows that $P_c = P_{c|C_0}$. Goodman[6] shows that the intensity I_N over a homogeneous region N with average reflectivity μ, defined as,

$$I_N = \sum_{(m,n)\in N} I_{mn} \; , \tag{36}$$

is gamma distributed, with the density function

$$p_{I_N}(I_N|\mu) = \frac{1}{\mu^{\nu}\Gamma(\nu)} I_N^{\nu-1} \exp(-I_N/\mu) I_{[0,\infty)}(I_N) \; , \tag{37}$$

where $\nu = \mathrm{card}(N) \times L$. Since the result will be the same for any general set N with parameter ν, and since both N_1 and N_0 have the same parameter ν, we will drop their subscripts and use the notation N. By analogy to Eq. (34), the probability of correct decision for the detection problem, taking $K = 2$, is given by

$$P_c = \int_0^{\infty} p_{I_N}(\sigma|\mu_1)\left[\int_0^{\sigma} p_{I_N}(\tau|\mu_0)\, \mathrm{d}\tau\right] \mathrm{d}\sigma \; . \tag{38}$$

In Appendix C, we show that the analytical expansion of this equation yields the same expression for P_e $(= 1 - P_c)$ as in Eq. (24). Hence the Type I detection problem is analogous to the detection of orthogonal signals in communication systems.

4.1.2 *Extension to K alternative pattern orientation and discrimination*

We now study the problem of object orientation and form discrimination from a set of K object patterns as shown in Fig. 8. We assume that $\mathrm{card}(C_i) = \mathrm{card}(C_j)$, and we will simply use the notation N in the following analysis to represent the differing pixel components.

By analogy to Eq. (34), the probability of correct detection among the set of K patterns is given by

$$P_c = \int_0^{\infty} p_{I_N}(\sigma|\mu_1)\left(\int_0^{\sigma} p_{I_N}(\tau|\mu_0)\, \mathrm{d}\tau\right)^{K-1} \mathrm{d}\sigma \; , \tag{39}$$

where the pdf of I_N was given in Eq. (37). As shown in Appendix D, expanding Eq. (39) analytically results in the following expression for P_c:

$$P_c = \frac{(K-1)!}{(\nu-1)!} \sum_{k=0}^{K-1} \sum_{(l_0, l_1, \ldots, l_{\nu-1})\in S_k} \times \frac{(-1)^k(\alpha_l + \nu - 1)!}{(K-k-1)!(1+kr)^{\nu}(k+r^{-1})^{\alpha_l}\beta_l} \; , \tag{40}$$

where

$$r = \mu_1/\mu_0 \; ,$$

$$\nu = \mathrm{card}(N) \times L \; ,$$

$$\alpha_l = \sum_{j=1}^{\nu-1} j l_j \; ,$$

$$\beta_l = \prod_{j=0}^{\nu-1} l_j!(j!)^{l_j} \; ,$$

and S_k is the set of all ν-tuples of nonnegative integers whose

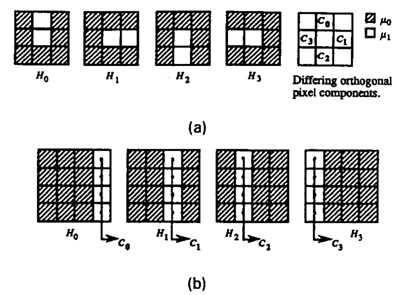

Fig. 8 (a) K alternative orientations of an object and (b) K alternative forms of an object, ($K=4$).

sum is k. The expression for P_c can be evaluated numerically. We note from Figs. 10 and 11 (Type I curves) that for fixed values of K and ν, $P_e(=1-P_c)$ gets smaller with increasing values of the contrast ratio r. We also note that for fixed values of r and ν, P_e increases with increasing values of K. This is expected, because an increase in K causes the detector decision to be made among a larger set of hypotheses. Thus, the probability of correct decision is reduced when all other factors are held constant.

4.1.3 *Gaussian approximation*

Consider the statistic I_N given by Eq. (36). Recall that each pixel intensity I_{mn} based on L looks is gamma distributed according to Eq. (5). Since the intensities $\{I_{mn}\}$ are statistically independent, it follows that the mean and variance of I_N are given by

$$E(I_N)=(\mathrm{card}(N)\times L)\times\mu=\nu\mu \ , \tag{41}$$

and

$$\sigma_{I_N}^2=\mathrm{card}(N)\times\sigma_{I_{mn}}^2=\nu\mu^2 \ , \tag{42}$$

respectively. It follows from the central limit theorem[18] that I_N converges in distribution to a Gaussian random variable $G\sim N(\nu\mu,\nu\mu^2)$ for large values of ν. That is,

$$P_{I_N}(I_N|\mu)\approx\frac{1}{\mu\sqrt{2\pi\nu}}\exp\left[-\frac{(I-\nu\mu)^2}{2\nu\mu^2}\right] \ , \quad \text{for large } \nu \ . \tag{43}$$

Substituting this equation into Eq. (39) results in the following approximation for the probability of a correct decision for large ν:

$$P_c\approx\int_0^\infty\frac{1}{\mu_1\sqrt{2\pi\nu}}\exp\left[-\frac{(\xi-\nu\mu_1)^2}{2\nu\mu_1^2}\right] \times\left[Q(-\sqrt{\nu})-Q\left(\frac{\xi-\nu\mu_0}{\mu_0\sqrt{\nu}}\right)\right]^{K-1} d\xi \ . \tag{44}$$

Here $Q(\cdot)$ is the Q-function defined as

$$Q(x)=\frac{1}{\sqrt{2\pi}}\int_x^\infty \exp(-\xi^2/2)\ d\xi \ . \tag{45}$$

Equation (44) can be evaluated numerically and is accurate to three decimal places for $\nu\geqslant 25$.

4.2 *Type II Problems*

Type II problems correspond to antipodal signaling problems in statistical communication theory. Only pattern discrimination problems fall into the Type II category. For example, the discrimination of patterns in sets 1, 2, and 3 of Fig. 6 are Type II problems. Here, we consider an object with two reflectivity levels μ_0 and μ_1 ($\mu_1>\mu_0$) under two hypotheses H_0 and H_1. We define the set N_1 as follows: $N_1=\{(m,n)$ dark pixels (μ_0) under H_1 that are different from the dark pixels under $H_0\}$. In this problem, the set N_0 as defined in Sec. 4.1 is empty. Again, we have $\nu=\mathrm{card}(N_1)\times L$.

Based on the analysis of Sec. 3.3, the decision rule for the maximum likelihood test is the same as in Eqs. (28), (29), and (30). The probability of error P_e is given by Eq. (32).

4.2.1 *Analogy to binary antipodal signals*

Consider the Type II problem in Fig. 6. Only pixels with average reflectivities that differ in the two forms being tested belong to the set N_1. Hence, deciding which of the two hypotheses H_0 or H_1 is true can be solely based on whether or not the pixels in N_1 are bright (H_0) or dark (H_1). Because the problem reduces to determining if the pixels in N_1 are bright or dark, it is analogous to the optimal detection of two equal-energy antipodal signals at the receiver end of a communication channel with additive noise. In fact, the error probability in Eq. (32) for pattern discrimination has the same form as the analogous problem in statistical communication theory.[29,30]

4.2.2 *Gaussian approximation*

Consider the statistic I_N (denoting N_1 by N) given by Eq. (36). Using the central limit theorem, the gamma pdf of I_N is approximated by a Gaussian pdf with mean $\nu\mu$ and variance $\nu\mu^2$ for large values of ν. Hence, we have

$$p_{I_N}(I_N|H_0)\approx\frac{1}{\mu_1\sqrt{2\pi\nu}}\exp\left[-\frac{(I-\nu\mu_1)^2}{2\nu\mu_1^2}\right] \ , \tag{46}$$

and

$$p_{I_N}(I_N|H_1)\approx\frac{1}{\mu_0\sqrt{2\pi\nu}}\exp\left[-\frac{(I-\nu\mu_0)^2}{2\nu\mu_0^2}\right] \ , \quad \text{for large } \nu \ . \tag{47}$$

Applying Eq. (21)(I^* is now replaced by I_N), direct integration of the conditional pdfs of I_N yields the following approximate expression for the probability of error:

$$P_e\approx\frac{1}{2}\left(1-Q\left\{\sqrt{\nu}\left[\frac{\ln(r)}{r-1}-1\right]\right\}+Q\left\{\sqrt{\nu}\left[\frac{\ln(r)}{1-r^{-1}}-1\right]\right\}\right) \tag{48}$$

for large ν, where $Q(\cdot)$ is the Q-function defined in Eq. (45).

The simple expression for P_e given by Eq. (48) closely approximates Eq. (32) for large ν and is accurate to three decimal places for $\nu \geqslant 25$.

4.3 *Type III Problems*

Type III problems correspond to biorthogonal signal detection problems in statistical communication theory. Recall that only pattern discrimination could fall into the class of Type II problems. We also noted that the problem of form discrimination from a set of four known patterns as depicted in Fig. 8(b) falls under a Type I problem. In general, form discrimination from a set of $K(\geqslant 4)$ known patterns may not be a Type I problem. We assume that $K \geqslant 4$ and that it is even. The detection problem is considered to be Type III when

1. a set of $K/2$ patterns forms a Type I problem
2. the set of the remaining $K/2$ patterns also forms a Type I problem
3. each pattern from the first set, together with a corresponding pattern from the second set, forms a Type II problem.

As an example, the pattern discrimination problem of Fig. 9 is a Type III problem. In fact, H_0 and H_1 are Type I; H_2 and H_3 are also Type I; H_0 and H_2 are Type II (detection based on N_0 being bright or dark); and H_1 and H_3 are Type II (detection based on N_1' being bright or dark).

We assume that $\mathrm{card}(N_i) = \mathrm{card}(N_j) = \mathrm{card}(N_1')$, and we will simply use the notation N by the same argument used for Type I problems. Since it was noted that Type I and Type II correspond to equal-energy orthogonal signals and equal-energy antipodal signals, respectively, it follows that Type III problems are analogous to equal-energy biorthogonal signal detection problems in statistical communication theory. The probability of correct detection[29] is given by

$$P_c = \int_0^\infty p_{I_N}(\sigma|\mu_1) \left[\int_0^\sigma p_{I_N}(\tau|\mu_0)\, d\tau \right]^{(K/2)-1} d\sigma \;, \tag{49}$$

where the pdf of I_N was given in Eq. (37). Expanding this equation results in the same expression for P_c as in Eq. (40), except that K is replaced by $K/2$:

$$P_c = \frac{(K/2-1)!}{(\nu-1)!} \sum_{k=0}^{k/2-1} \sum_{(l_0, l_1, \ldots, l_{\nu-1}) \in S_k} \times \frac{(-1)^k (\alpha_l + \nu - 1)!}{(K/2-k-1)!(1+kr)^\nu (k+r^{-1})^{\alpha_l} \beta_l} \;, \tag{50}$$

where

$$r = \mu_1/\mu_0 \;,$$

$$\nu = \mathrm{card}(N) \times L \;,$$

$$\alpha_l = \sum_{j=1}^{\nu-1} j\, l_j \;,$$

$$\beta_l = \prod_{j=0}^{\nu-1} l_j!(j!)^{l_j} \;,$$

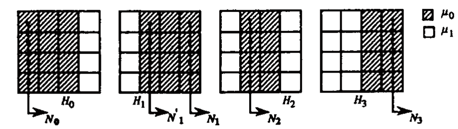

Fig. 9 *K* alternative form discrimination ($K=4$).

and S_k is the set of all ν-tuples of nonnegative integers whose sum is k. The Gaussian-based approximation of P_c is also given by Eq. (44) with K replaced by $K/2$:

$$P_c \approx \int_0^\infty \frac{1}{\mu_1\sqrt{2\pi\nu}} \exp\left[-\frac{(\xi - \nu\mu_1)^2}{2\nu\mu_1^2} \right] \times \left[Q(-\sqrt{\nu}) - Q\left(\frac{\xi - \nu\mu_0}{\mu_0\sqrt{\nu}} \right) \right]^{K/2-1} d\xi \tag{51}$$

for large ν, where $Q(\cdot)$ is the Q-function defined previously.

5 Results and Comparison with Human Visual Detection

5.1 *Detector Performance for Type I, II, and III Problems*

We have shown that many problems of pattern recognition of binary images corrupted by speckle can be put into one of three classes for which error probability analyses were presented. This generalization makes the design of optimal statistical tests for pattern recognition problems straightforward. The probability of error equations developed for the various classes have been implemented as FORTRAN programs on a Sun workstation. A comparison between the detectors performance in terms of P_e for Type I and II problems is illustrated in Fig. 10. For Type I, P_e is lower than that of Type II with the difference being more significant for low values of the contrast ratio r. This can be justified by noting that there are two sets N_0 and N_1 of differing pixels between the two patterns for Type I problems, and only one set N of differing pixels for Type II problems, which makes the probability of error higher for Type II problems for fixed object size, contrast ratio, and number of SAR looks. Figure 11 shows that P_e for Type III is lower than that of Type I. This is expected because, for fixed values of ν and r, the probability of error for Type III problems corresponds to that of Type I problems with half the number of Type I hypotheses K being used. Thus, Type II detection problems are the most demanding in terms of image size in pixels, contrast ratio, and number of SAR looks for good detection performance, and thus make good test problems for object detection in SAR images.

5.2 *Comparison with Human Visual Detection Performance*

Korwar and Pierce[15,16] have developed a theoretical model for human observer's detection in images corrupted by speckle. They noted from theoretical calculations and psychological experiments that grating orientation for human observers becomes more easily discriminated as the grating lines become wider because the eye sums horizontally over

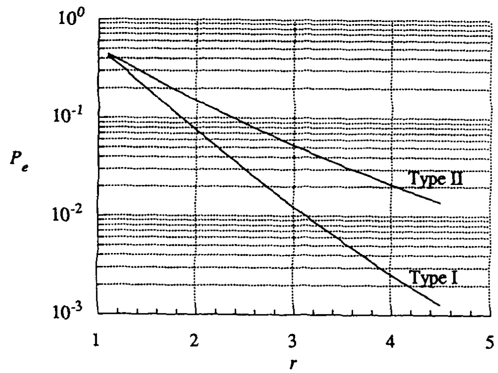

Fig. 10 Probability of error comparison between Type I and II ($\nu=9$, $K=2$).

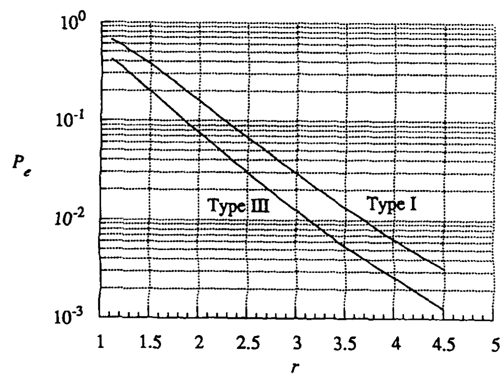

Fig. 11 Probability of error comparison between Type I and III ($\nu=9$, $K=4$).

the width of each line.[16] For machine detection, however, we found that the optimal detector performance was independent of the line thickness d. For example, an L-look grating with lines that are two pixels wide and size $M \times N$ (in resolution cells) results in the same P_e as a grating with lines one pixel wide and with the same number of looks L and size $M \times N$. Also, for the same r and ν, the human observer's performance may be different when discriminating between two forms from different sets as shown in Table 2. On the other hand, when all other parameters are fixed, the shape of the object has no effect on machine detection performance. Machine detectors will have the same P_e for form discrimination from various sets (for instance, sets 2 and 3 in Fig. 6), provided that the two forms in each set have an equal number of different intensity pixels card(N_1). Finally, it is noted that the overall performance of the machine optimal detection test is better than that of the human observer based on Korwar and Pierce estimates of human observers performance. Table 3 shows that the probability of correct detection for machine detection is higher than the upper bounds on the human visual detector's P_c obtained by Korwar and Pierce[15,16] from psychological experiments. Hence, machine detection has a better performance than human detection even when the discrimination model for the human visual system is based on the most favorable assumptions.[15]

Table 2 Korwar and Pierce results for form discrimination by human observers.

r (dB)	ν	P_c (set 2, Fig. 1)	P_c (set 3, Fig. 1)
1	150	0.78	0.84
	153	0.86	0.82
	250	0.85	0.80
	500	0.91	0.92

Table 3 Comparison between human and machine detection performance. We tabulate the upper bound P_c for human detection obtained by Korwar and Pierce.[15,16]

r (dB)	ν	P_c (set 2 Fig. 1)		P_c (orientation, Fig. 1(a))		P_c (orientation, Fig. 1)	
		Human	Machine	Human	Machine	Human	Machine
1	150	0.86	0.919	0.91	0.977	—	0.941
	153	0.90	0.922	0.90	0.978	0.79	0.942
	208	0.88	0.954	0.92	0.992	0.87	0.968
	250	0.92	0.971	0.99	0.995	0.89	0.991
	500	0.96	0.996	1.0	0.999	0.99	0.999
3	18	0.92	0.927	Human data unavailable			
	25	0.91	0.956				
	306	1.0	1.0				
5	1	0.74	0.701				
	4	0.84	0.868				

6 Summary and Conclusions

In this paper, we developed optimal statistical tests based on intensity measurements from SAR systems for the pattern recognition problems of object orientation-determination and form discrimination. In particular, we examined the detection problems of grating orientation for gratings with lines that are one pixel wide and more generally d pixels wide and discrimination between two alternative forms. We developed decision rules and probability of error formulas for these decision rules. Based on these analyses, we classified a broad range of pattern recognition problems into three categories:

1. Type I, under which both object orientation-determination and pattern discrimination problems could fall. These problems correspond to orthogonal signal detection problems.
2. Type II, under which only pattern discrimination problems could fall. These problems correspond to antipodal signal detection problems.
3. Type III, under which only pattern discrimination problems with K hypotheses ($K \geq 4$ and even) could fall. These problems correspond to biorthogonal signal detection problems.

For each class, we derived a decision rule based solely on intensity measurements of the returned signal. We found that only the different pixel components between the object taking on the reflectivities (μ_0 and μ_1) under the various hypotheses are used in decision making, and thus about half of the intensity pixel measurements are discarded. We also derived for each class mathematical relations between the probability of error and the number of SAR looks L, the image contrast ratio r, and the size (in resolution pixels) of the object being considered. Using Gaussian approximation, we obtained simpler and more computationally efficient formulas for P_e that are close to the exact ones up to three decimal places for $\nu \geq 25$. The classification of pattern recognition problems and these probability of error equations make the design of object detection procedures for SAR images straightforward.

We noted from the probability of error equations that it is not possible to characterize the detector performance by a single parameter. We found that the probability of error is related only to the contrast ratio r and to two parameters ν and η that are proportional to the number of SAR looks L and to the number of differing pixels between the patterns to be distinguished. Consequently, for a fixed value of r, two different detection problems with the same values of ν and η have exactly the same probability of error. This leads to the interesting results that grating orientation detection is independent of the grating line thickness d, and that form discrimination is independent of the shape of the object being considered—a result that is not true for detection by a human observer. It was also found that P_e decreases with an increase in r, ν, and η, which means that pattern orientation-determination and discrimination become easier as the contrast ratio and the number of differing pixels between the patterns become higher.

We also showed that Type I, II, and III detection problems are analogous to the problems of optimal detection of orthogonal, antipodal, and biorthogonal signals, respectively, in statistical communications theory. Following this analogy to statistical communication theory, we developed formulas for the probability of correctly determining the orientation of K patterns and discriminating among K alternative forms. After comparing the performance of the tests for Type I, II, and III problems, we found that Type II problems are the most demanding in terms of image size, contrast ratio, and number of SAR looks for detection performance, and thus make good test problems for object detection in SAR images.

We also provided a comparison between the results that we obtained for machine detection and those obtained by Korwar and Pierce[15,16] for human observers. For machine detection, grating orientation-determination was independent of the grating line width d, whereas grating orientation for human observers becomes more easily discriminated as d gets larger. We also found that, unlike human visual detection, for fixed values of r, ν, and η, the shape of the object has no effect on machine detection performance. We also noticed through numerical computations that the overall performance of the machine optimal detection test is better than that of the human observer.

Although the images treated in this paper were binary images consisting of only two reflectivity levels, extensions can be made to other forms of images. For images with multiple intensity levels, we obtain a problem analogous to that of multilevel, as opposed to binary, quantization in statistical communication theory.[29] However, due to the wide dynamic range[31] yet low information content per pixel in microwave images,[21,22] the binary image model is reasonable in many applications.

Finally, we mention that the assumptions made about speckle in SAR images could also be made about speckle in images generated by other coherent systems, and thus the analysis and results of this paper could serve as a basis for detection problems in other coherent imaging systems where the speckle phenomenon is present, such as ultrasonic, laser, and sonar imaging systems.

7 Appendix A: Derivation of the pdf of I^* Conditioned on H_0 [Eqs. (17), (18), and (19)]

The gamma distribution of a pixel intensity based on L looks has the following characteristic function[18]:

$$\phi_{I^*}(w) = E[\exp(jwI^*)] = (1 - j\mu w)^{-L} \ . \tag{52}$$

This expression is obtained by an inverse Fourier transformation of Eq. (5). The characteristic function of the statistic I^* is

$$\begin{aligned}\phi_{I^*|H_0}(w) &= E_0[\exp(jwI^*)] \\ &= E_0\left\{\exp\left[jw\left(\sum_{m\ \mathrm{odd}}\ \sum_{n\ \mathrm{even}} I_{mn} - \sum_{m\ \mathrm{even}}\ \sum_{n\ \mathrm{odd}} I_{mn}\right)\right]\right\} \\ &= \prod_{m\ \mathrm{odd}}\ \prod_{n\ \mathrm{even}} E_0[\exp(jwI_{mn})] \\ &\quad \times \prod_{m\ \mathrm{even}}\ \prod_{n\ \mathrm{odd}} E_0[\exp(-jwI_{mn})] \ ,\end{aligned} \tag{53}$$

using the fact that the intensities $\{I_{mn}\}$ are conditionally independent. After substituting in Eq. (52), we obtain

$$\phi_{I^*|H_0}(w) = (1 - jw\mu_1)^{-\nu L}(1 + jw\mu_0)^{-\eta L} , \qquad (54)$$

where ν and η are the constants in Table 1. Taking the inverse Fourier transform of Eq. (54) and using a partial fraction expansion[32] yields

$$p_0(I^*) = \mu_1^{-\nu}\mu_0^{-\eta}\left[\sum_{k=0}^{\nu-1} a_k I^{*k} \exp(-I^*/\mu_1) I_{[0,\infty)}(I^*) + \sum_{k=0}^{\eta-1} b_k(-I^*)^k \exp(I^*/\mu_0) I_{(-\infty,0)}(I^*)\right] , \qquad (55)$$

where

$$a_k = \left.\frac{[(-jw + 1/\mu_0)^{-\eta}]^{(\nu-k-1)}}{(\nu-k-1)!k!}\right|_{jw=-1/\mu_1} , \qquad (56)$$

and

$$b_k = \left.\frac{(-1)^{\eta-k-1}[(jw + 1/\mu_1)^{-\nu}]^{(\eta-k-1)}}{(\eta-k-1)!k!}\right|_{jw=1/\mu_0} , \qquad (57)$$

with the superscripts in parentheses denoting derivative orders. It follows from the direct evaluations of Eqs. (56) and (57) that

$$a_k = \frac{1}{k!}\binom{\eta+\nu-k-2}{\eta-1}\left(\frac{1}{\mu_1}+\frac{1}{\mu_0}\right)^{-\eta-\nu+k+1} , \qquad (58)$$

and

$$b_k = \frac{1}{k!}\binom{\eta+\nu-k-2}{\nu-1}\left(\frac{1}{\mu_1}+\frac{1}{\mu_0}\right)^{-\eta-\nu+k+1} . \qquad (59)$$

8 Appendix B: Generalized Marcum Q-Function and Error Probability for Grating Orientation [Eqs. (22) and (23)]

Let us first consider the definite integral

$$f(I_t) = \int_{I_t}^{\infty} \frac{\xi^{N-1} \exp(-\xi/\mu)}{\mu^N \Gamma(N)}\, d\xi , \qquad (60)$$

where $I_t \geqslant 0$ and $\Gamma(N)$ is the gamma function and is equal to $(N-1)!$ for integer arguments. Using successive integrations by parts, the definite integral $f(I_t)$ has the evaluation[33]

$$f(I_t) = \psi_{N-1}(I_t/\mu) , \qquad (61)$$

where, for positive integer M,

$$\psi_M(x) = \exp(-x)\sum_{m=0}^{M} \frac{x^m}{m!} . \qquad (62)$$

Helstrom[34] gives an approximation to $\psi_M(x)$ as

$$\psi_M(x) \approx \frac{x^{M+1}\exp(-x)}{M!(x-M)} \quad \text{for } x \gg M . \qquad (63)$$

We now relate the definite integral of Eq. (60) to the generalized Marcum Q-function $Q_N(\alpha,\beta)$. Shnidman[26] gives a power series expression for the generalized Marcum Q-function as

$$Q_N(\alpha,\beta) = P_N(0.5\alpha^2/N, 0.5\beta^2) , \qquad (64)$$

where

$$P_N(x,y) = \sum_{n=0}^{N-1} \exp(-y)\frac{y^n}{n!} + \sum_{n=N}^{\infty} \exp(-y)\frac{y^n}{n!} \times \left[1 - \sum_{k=0}^{n-N} \exp(-Nx)\frac{(Nx)^k}{k!}\right] . \qquad (65)$$

Examination of Eqs. (61), (62), (64), and (65) shows that the definite integral of Eq. (60) is related to the generalized Marcum Q-function according to

$$\int_{I_t}^{\infty} \frac{\xi^{N-1}\exp(-\xi/\mu)}{\mu^N\Gamma(N)}\, d\xi = Q_N[0,(2I_t/\mu)^{1/2}] , \quad I_t \geqslant 0 . \qquad (66)$$

Applying Eq.(21) and using the expression for the conditional pdf $p_0(I^*)$ from Eq. (17) and the dual expression for $p_1(I^*)$ yields

$$\begin{aligned} P_e = \frac{1}{2}\Bigg\{ & \mu_1^{-\nu}\mu_0^{-\eta}\Bigg[\sum_{k=0}^{\nu-1} a_k \int_{-\infty}^{I_t} \xi^k \exp(-\xi/\mu_1) I_{[0,\infty)}(\xi)\, d\xi \\ & + \sum_{k=0}^{\eta-1} b_k \int_{-\infty}^{I_t} (-\xi^k) \exp(\xi/\mu_0) I_{(-\infty,0)}(\xi)\, d\xi\Bigg] \\ & + \mu_0^{-\nu}\mu_1^{-\eta}\Bigg[\sum_{k=0}^{\nu-1} a_k \int_{I_t}^{\infty} \xi^k \exp(-\xi/\mu_0) I_{[0,\infty)}(\xi)\, d\xi \\ & + \sum_{k=0}^{\eta-1} b_k \int_{I_t}^{\infty} (-\xi^k) \exp(\xi/\mu_1) I_{(-\infty,0)}(\xi)\, d\xi\Bigg]\Bigg\} . \end{aligned} \qquad (67)$$

For the case when $I_t \geqslant 0$ (or $\nu \geqslant \eta$), Eq. (67) simplifies to

$$\begin{aligned} P_e = \frac{1}{2}\Bigg\{ & \mu_1^{-\nu}\mu_0^{-\eta}\Bigg[\sum_{k=0}^{\nu-1} a_k \int_{0}^{I_t} \xi^k \exp(-\xi/\mu_1)\, d\xi \\ & + \sum_{k=0}^{\eta-1} b_k \int_{0}^{\infty} (-\xi^k) \exp(-\xi/\mu_0)\, d\xi\Bigg] \\ & + \mu_0^{-\nu}\mu_1^{-\eta} \sum_{k=0}^{\nu-1} a_k \int_{I_t}^{\infty} \xi^k \exp(-\xi/\mu_0)\, d\xi\Bigg\} . \end{aligned} \qquad (68)$$

Using Eq. (66), Eq. (68) simplifies further to

$$P_e=\frac{1}{2}\Bigg[\mu_1^{-\nu}\mu_0^{-\eta}\Bigg(\sum_{l=0}^{\nu-1}a_l\mu_1^{l+1}l!\{1-Q_{l+1}$$

$$\times[0,(2|I_t|/\mu_1)^{1/2}]\}+\sum_{j=0}^{\eta-1}b_j\mu_0^{j+1}j!\Bigg)$$

$$+\mu_0^{-\nu}\mu_1^{-\eta}\sum_{l=0}^{\nu-1}a_l\mu_0^{l+1}l!Q_{l+1}[0,(2|I_t|/\mu_0)^{1/2}]\Bigg]. \quad (69)$$

Similarly, for the case when $I_t<0$ (or $\nu<\eta$), P_e is given by

$$P_e=\frac{1}{2}\Bigg[\mu_0^{-\nu}\mu_1^{-\eta}\Bigg(\sum_{j=0}^{\eta-1}b_j\mu_1^{j+1}j!\{1-Q_{j+1}$$

$$\times[0,(2|I_t|/\mu_1)^{1/2}]\}+\sum_{l=0}^{\nu-1}a_l\mu_0^{l+1}l!\Bigg)$$

$$+\mu_1^{-\nu}\mu_0^{-\eta}\sum_{j=0}^{\eta-1}b_j\mu_0^{j+1}j!Q_{j+1}[0,(2|I_t|/\mu_0)^{1/2}]\Bigg]. \quad (70)$$

Using the expressions of a_k and b_k from Eqs. (18) and (19) and making the change of variables $k=\nu-l-1$ and $k=\eta-j-1$ yields the final expression for P_e as in Eqs. (22) and (23).

9 Appendix C: Analytical Expansion of Eq. (38)

Substituting Eq. (37) into Eq. (38) results in

$$P_c=\int_0^\infty p_{IN}(\sigma|\mu_1)\left[\int_0^\sigma\frac{1}{\mu_0^\nu\Gamma(\nu)}\tau^{\nu-1}\exp(-\tau/\mu_0)\,d\tau\right]d\sigma\ , \quad (71)$$

or, using Eq. (66) from Appendix B,

$$P_c=\int_0^\infty p_{IN}(\sigma|\mu_1)\{1-Q_\nu[0,(2\sigma/\mu_0)^{1/2}]\}\ d\sigma \quad (72)$$

$$=1-\int_0^\infty p_{IN}(\sigma|\mu_1)Q_\nu[0,(2\sigma/\mu_0)^{1/2}]\ d\sigma\ , \quad (73)$$

which implies that

$$P_e=1-P_c=\int_0^\infty p_{IN}(\sigma|\mu_1)Q_\nu[0,(2\sigma/\mu_0)^{1/2}]\ d\sigma\ , \quad (74)$$

or, after substituting in Eq. (37) and using the series expansion of the generalized Marcum Q-function from Eq. (65) in Appendix B,

$$P_e=\int_0^\infty\frac{1}{\mu_1^\nu\Gamma(\nu)}\sigma^{\nu-1}\exp(-\sigma/\mu_1)$$

$$\times\left[\sum_{k=0}^{\nu-1}\frac{1}{k!}\exp(-\sigma/\mu_0)\left(\frac{\sigma}{\mu_0}\right)^k\right]d\sigma \quad (75)$$

$$=\frac{1}{\mu_1^\nu(\nu-1)!}\sum_{k=0}^{\nu-1}\frac{1}{k!\mu_0^k}\int_0^\infty\sigma^{\nu-k-1}$$

$$\times\exp\left[-\left(\frac{1}{\mu_0}+\frac{1}{\mu_1}\right)\sigma\right]d\sigma \quad (76)$$

$$=\frac{1}{\mu_1^\nu(\nu-1)!}\sum_{k=0}^{\nu-1}\frac{(\nu+k-1)!}{k!\mu_0^k}\left(\frac{1}{\mu_0}+\frac{1}{\mu_1}\right)^{-\nu-k}\ . \quad (77)$$

Setting $r=\mu_1/\mu_0$, it follows that

$$P_e=(1+r)^{-\nu}\sum_{k=0}^{\nu-1}\binom{\nu+k-1}{\nu-1}(1+r^{-1})^{-k}\ . \quad (78)$$

Making the change of variable $j=\nu-k-1$ yields the probability of error expression in Eq. (24).

10 Appendix D: Probability of Correct Detection Among K Object Patterns [Eq. (40)]

Substituting Eq. (37) into Eq. (39) results in

$$P_c=\int_0^\infty p_{IN}(x|\mu_1)\left(\int_0^x\frac{1}{\mu_0^\nu(\nu-1)!}y^{\nu-1}\exp(-y/\mu_0)\,dy\right)^{K-1}dx\ , \quad (79)$$

or, after using Eq. (66) from Appendix B,

$$P_c=\int_0^\infty p_{IN}(x|\mu_1)\{1-Q_\nu[0,(2x/\mu_0)^{1/2}]\}^{K-1}\ dx\ . \quad (80)$$

Using the binomial formula,[35] and after interchanging summation and integration, we obtain

$$P_c=\sum_{k=0}^{K-1}(-1)^k\binom{K-1}{k}\int_0^\infty p_{IN}(x|\mu_1)\{Q_\nu[0,(2x/\mu_0)^{1/2}]\}^k\ dx\ , \quad (81)$$

or, after using the series expansion of the generalized Marcum Q-function in Eq. (65) from Appendix B,

$$P_c=\sum_{k=0}^{K-1}(-1)^k\binom{K-1}{k}\int_0^\infty p_{IN}(x|\mu_1)$$

$$\times\left[\sum_{l=0}^{\nu-1}\frac{1}{l!}\exp(-x|\mu_0)\left(\frac{x}{\mu_0}\right)^l\right]^k dx\ , \quad (82)$$

which, after applying the multinomial formula,[35] can be written as

$$P_c=\sum_{k=0}^{K-1}(-1)^k\binom{K-1}{k}\int_0^\infty p_{I_N}(x|\mu_1)\sum_{l_k}\times\left\{\frac{k!\prod_{j=0}^{\nu-1}\left[\frac{1}{j!}\exp(-x/\mu_0)\left(\frac{x}{\mu_0}\right)^j\right]^{l_j}}{\prod_{i=0}^{\nu-1}l_i!}\right\}\mathrm{d}x\ , \tag{83}$$

where Σ_{l_k} is taken over all nonnegative integers $l_0,l_1,\ldots,l_{\nu-1}$ for which

$$\sum_{j=0}^{\nu-1}l_j=k\ .$$

After using Eq. (37) for $p_{I_N}(x|\mu_1)$ and interchanging summation and integration, we obtain

$$P_c=\sum_{k=0}^{K-1}\sum_{l_k}\left[\frac{(-1)^k(K-1)!}{(K-k-1)!\prod_{i=0}^{\nu-1}l_i!}\right]\int_0^\infty\frac{1}{\mu_1^\nu(\nu-1)!}x^{\nu-1}\times\exp(-x/\mu_1)\left\{\prod_{j=0}^{\nu-1}\left[\frac{1}{j!}\exp(-x/\mu_0)\left(\frac{x}{\mu_0}\right)^j\right]^{l_j}\right\}\mathrm{d}x\ . \tag{84}$$

This implies that

$$P_c=\frac{1}{(\nu-1)!}\sum_{k=0}^{K-1}\sum_{l_k}\left[\frac{(-1)^k(K-1)!}{(K-k-1)!\mu_1^\nu\prod_{i=0}^{\nu-1}l_i!(i!)^{l_i}\mu_0^{il_i}}\right]\times\int_0^\infty x^{\nu-1}\exp(-x/\mu_1)\left[\prod_{i=0}^{\nu-1}\exp(-xl_i/\mu_0)x^{il_i}\right]\mathrm{d}x \tag{85}$$

$$=\frac{1}{(\nu-1)!}\sum_{k=0}^{K-1}\sum_{l_k}\left[\frac{(-1)^k(K-1)!}{(K-k-1)!\mu_1^\nu\prod_{i=0}^{\nu-1}l_i!(i!)^{l_i}\mu_0^{il_i}}\right]\times\int_0^\infty x\exp\left(\nu-1+\sum_{i=1}^{\nu-1}il_i\right)\exp\left[-x\left(\frac{1}{\mu_1}+\frac{k}{\mu_0}\right)\right]\mathrm{d}x \tag{86}$$

$$=\frac{1}{(\nu-1)!}\sum_{k=0}^{K-1}\sum_{l_k}\frac{(-1)^k(K-1)!}{(K-k-1)!\mu_1^\nu\prod_{i=0}^{\nu-1}l_i!(i!)^{l_i}\mu_0^{il_i}}\times\frac{\left(\nu-1+\sum_{i=1}^{\nu-1}il_i\right)!}{\left(\frac{1}{\mu_1}+\frac{k}{\mu_0}\right)\exp\left(\nu+\sum_{i=1}^{\nu-1}il_i\right)} \tag{87}$$

$$=\frac{(K-1)!}{(\nu-1)!}\sum_{k=0}^{K-1}\sum_{l_k}\frac{(-1)^k\left(\nu-1+\sum_{i=1}^{\nu-1}il_i\right)}{(K-k-1)!\prod_{i=0}^{\nu-1}l_i!(i!)^{l_i}}\times\frac{1}{\mu_1^\nu\mu_0^{\left(\sum_{i=1}^{\nu-1}il_i\right)}\left(\frac{1}{\mu_1}+\frac{k}{\mu_0}\right)^\nu\left(\frac{1}{\mu_1}+\frac{k}{\mu_0}\right)^{\left(\sum_{i=1}^{\nu-1}il_i\right)}} \tag{88}$$

$$=\frac{(K-1)!}{(\nu-1)!}\sum_{k=0}^{K-1}\sum_{l_k}\times\left(\frac{(-1)^k\left(\nu-1+\sum_{i=1}^{\nu-1}il_i\right)}{(K-k-1)!(1+kr)^\nu(k+r^{-1})^{\left(\sum_{i=1}^{\nu-1}il_i\right)}\prod_{i=0}^{\nu-1}l_i!(i!)^{l_i}}\right),$$

where $r=\mu_1/\mu_0$. After setting

$$\alpha_l=\sum_{i=1}^{\nu-1}il_i$$

and

$$\beta_l=\prod_{i=0}^{\nu-1}l_i!(i!)^{l_i}\ ,$$

we obtain the final expression for P_c as given in Eq.(40).

Acknowledgment

This work was supported by NSF Research Initiation Award MIP-9010834 and a David Ross Grant.

References

1. J. P. Fitch, *Synthetic Aperture Radars*, Springer-Verlag, New York (1988).
2. J. G. Abbott and F. L. Thurstone, "Acoustic speckle: theory and experimental analysis," *Ultrason. Imag.* **1**, 303–324 (1979).
3. C. B. Burckhardt, "Speckle in ultrasound B-mode scans," *IEEE Trans. Sonics and Ultrasonics* **Su-25**(3), 1–6 (1978).
4. R. F. Wagner, S. W. Smith, J. M. Sandrik, and H. Lopez, "Statistics of speckle in ultrasound B-scans," *IEEE Trans. Sonics and Ultrasonics* **30**(3), 156–163 (1983).
5. J. W. Goodman, *Statistical Optics*, Wiley-Interscience, New York (1985).
6. J. W. Goodman, "Statistical properties of laser speckle patterns," *Laser Speckle and Related Phenomena*, 2d. ed., J. C. Dainty, Ed., Springer-Verlag, New York (1984).

7. H. H. Arsenault, "Information extraction from images degraded by speckle," *Proc. IGARSS 87 Symp.*, pp. 1317–1322 (1987).
8. A. Kozma and C. R. Christensen, "Effects of speckle on resolution," *J. Opt. Soc. Am.* **66**, 1257–1267 (1976).
9. L. J. Porcello, N. G. Massey, R. B. Innes, and J. M. Marks, "Speckle reduction in synthetic aperture radar," *J. Opt. Soc. Am.* **66**, 1305–1311(1976).
10. J. S. Lee, "A simple smoothing algorithm for synthetic aperture radar images," *IEEE Trans. Sys. Man Cyber.* **SMC-13**(1), 1311–1339 (1983).
11. J. S. Lee, "Statistical modelling and suppression of speckle in synthetic aperture radar images," *Proc. IGARSS 87 Symp.*, pp. 1331–1339 (1987).
12. A. C. Bovik and D. C. Munson, Jr., "Optimal detection of object boundaries in uncorrelated speckle," *Opt. Eng.* **25**(11), 1246–1252 (1986).
13. P. A. Kelly, H. Derin, and K. Hartt, "Adaptive segmentation of speckled images using a hierarchical random field model," *IEEE Trans. Acoust. Speech Sig. Proc.* **36**, 1628–1641 (Oct.1988).
14. H. Derin, P. A. Kelly, G. Vezina, and S. G. Labitt, "Modeling and segmentation of speckled images using complex data," *IEEE Trans. Geosci. Rem. Sens.* **28**(1), 76–87 (Jan. 1990).
15. V. N. Korwar and J. R. Pierce, "Discrimination of form in images corrupted by speckle," *Appl. Opt.* **20**(2), 320–325 (1981).
16. V. N. Korwar and J. R. Pierce, "Detection of gratings and small features in images corrupted by speckle," *Appl. Opt.* **20**(2), 312–319 (1981).
17. R. V. Ostrovityanov and F. A. Basalov, *Statistical Theory of Extended Radar Targets*, Artech House, Dedham, Massachusetts (1985).
18. A. Papoulis, *Probability, Random Variables, and Stochastic Processes*, 3rd ed., McGraw-Hill, New York (1991).
19. P. Billingsley, *Probability and Measure*, John Wiley & Sons, New York (1979).
20. F. T. Ulaby, R. K. Moore, and A. K. Fung, *Microwave Remote Sensing*, Vol. 2, Artech House, Dedham, Massachusetts (1982).
21. M. R. Bell, "Information theory and radar: mutual information and the design and analysis of radar waveforms and systems," PhD Thesis, California Institute of Technology, Pasadena (1988).
22. V. S. Frost and K. S. Shanmugan, "The information content of synthetic aperture radar images of terrain," *IEEE Trans. Aerospace Electron. Syst.* **AES-19**(5), 768–774 (1983).
23. R. K. Moore, "Tradeoff between picture element dimensions and noncoherent averaging in sidelooking radar," *IEEE Trans. Aerospace Electron. Syst.* **AES-15**, 697–708 (Sep. 1979).
24. J. S. Lim and H. Nawab, "Techniques for speckle noise removal," *Opt. Eng.* **20**(3),472–480 (1981).
25. H. V. Poor, *An Introduction to Signal Detection and Estimation*, Springer-Verlag, New York (1988).
26. D. A. Shnidman, "The calculation of the probability of detection and the generalized Marcum Q-function," *IEEE Trans. Inf. Theory* **35**(2), 389–400 (1989).
27. D. A. Shnidman, "Efficient evaluation of probabilities of detection and the generalized Q-function," *IEEE Trans. Inf. Theory* **IT-22**, 746–751(1976).
28. G. M. Dillard, "Recursive computation of the generalized Q-function," *IEEE Trans. Aerospace Electron. Syst.* **AES-9**, 614–615(1973).
29. J. M. Wozencraft and I. M. Jacobs, *Principles of Communication Engineering*, John Wiley & Sons, New York (1965).
30. J. A. Cooper, Jr., and C. R. McGillem, *Modern Communication and Spread Spectrum*, McGraw-Hill, New York (1986).
31. B. D. Steinberg and H. M. Subbaram, *Microwave Imaging Techniques*, Wiley Interscience, New York (1991).
32. C. R. Wylie, *Advanced Engineering Mathematics*, McGraw-Hill, New York (1975).
33. M. Abramowitz and I. A. Stegun, *Handbook of Mathematical Functions*, Appl. Math. Series 55, National Bureau of Standards, U.S. Govt. Printing Office, Washington, DC (1964).
34. C. W. Helstrom, *Statistical Theory of Signal Detection*, 2nd ed., pp. 218–219, Pergamon, New York (1968).
35. M. R. Spiegel, *Mathematical Handbook of Formulas and Tables*, McGraw-Hill, New York (1990).

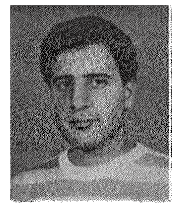

Jihad S. Daba received the BSEE degree in electrical engineering from the University of Houston, Texas, in 1988. He received his MSEE degree in electrical engineering from Purdue University, West Lafayette, Indiana, in 1990. He is presently working toward the PhD degree in electrical engineering at Purdue, where he is the recipient of a David Ross Grant. His research interests are in the area of coherent imaging and synthetic aperture radar, with an emphasis on object detection, pattern recognition, and estimation problems in speckled images.

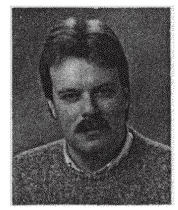

Mark R. Bell received the BS degree in electrical engineering from California State University Long Beach in 1981 and the MS and PhD degrees in electrical engineering from the California Institute of Technology (Caltech) in 1982 and 1988. While at Caltech from 1984 through 1988, he was a Howard Hughes Doctoral Fellow. From 1979 through 1989, he was employed by Hughes Aircraft Company, Fullerton, California. From 1981 through 1989 he was affiliated with the Radar Systems Laboratory, where he held the positions of member of the technical staff and staff engineer and did work in the areas of radar signal processing, electromagnetic scattering, radar systems analysis, and radar target recognition. In 1989, he joined the faculty of the School of Electrical Engineering at Purdue University, where he does research in information theory, source coding, radar signal processing, and scattering from rough surfaces. Dr. Bell was the recipient of the 1992 Ruth and Joel Spira Outstanding Teaching Award in the School of Electrical Engineering at Purdue.